

# Quantum calculations of $\text{H}_2\text{-H}_2$ collisions: from ultracold to thermal energies

Goulven Quéméner, Naduvalath Balakrishnan  
*Department of Chemistry, University of Nevada Las Vegas,  
Las Vegas, NV 89154, United States of America*  
(Dated: October 30, 2018)

We present quantum dynamics of collisions between two para- $\text{H}_2$  molecules from low ( $10^{-3}$  K) to high collision energies (1 eV). The calculations are carried out using a quantum scattering code that solves the time-independent Schrödinger equation in its full dimensionality without any decoupling approximations. The six-dimensional potential energy surface for the  $\text{H}_4$  system developed by Boothroyd et al. [J. Chem. Phys. **116**, 666 (2002)] is used in the calculations. Elastic, inelastic and state-to-state cross sections as well as rate coefficients from  $T = 1$  K to 400 K obtained from our calculations are compared with available experimental and theoretical results. Overall, good agreement is obtained with previous studies.

PACS numbers:

## I. INTRODUCTION

Collisions between molecules are fundamental processes which take place in many areas of physics and chemistry. Molecular collisions are prevalent in the interstellar medium, in the atmospheres of planets, in combustion chemistry and in many other chemical and industrial processes. Being the simplest neutral molecule - molecule system, the  $\text{H}_2\text{-H}_2$  system has served as a prototype for accurate calculations of tetratomic potential energy surfaces (PESs) as well as accurate quantum dynamics treatment of diatom - diatom collisions. Since  $\text{H}_2$  is the most abundant molecular species in the universe, collisions between  $\text{H}_2$  molecules leading to excitation and de-excitation of their rovibrational levels continue to be a topic of considerable interest in interstellar chemistry. However, an accurate calculation of rovibrational energy transfer rate coefficients in  $\text{H}_2\text{-H}_2$  collisions for temperatures relevant to astrophysical environments is still a challenging problem. In recent years, due to the success in creating dense samples of ultracold molecules in magneto-optical traps, atomic and molecular collisions in cold and ultracold gases have attracted considerable experimental and theoretical attention [1, 2, 3, 4, 5, 6, 7, 8]. These unusual systems provide a fascinating opportunity to investigate atomic and molecular processes at temperatures close to absolute zero where the collisional outcomes are dramatically influenced by quantum effects. Recent studies of atom - diatom inelastic and reactive collisions at temperatures close to absolute zero have shown that such processes may occur with significant rate coefficients at ultracold temperatures [9, 10, 11, 12, 13, 14, 15, 16, 17, 18, 19]. The  $\text{H}_2\text{-H}_2$  system serves as an ideal prototype to investigate molecule - molecule collisions at ultracold temperatures.

Several PESs of the  $\text{H}_4$  system have been calculated in the literature. Some of the earlier studies treated the diatomic molecules as a rigid rotor (RR) as in the work of Zarur and Rabitz (ZR) [20], Schaefer and Köhler (SK) [21], Diep and Johnson (DJ) [22], and the recent

study of Patkowski et al. [23]. Some of these PESs have been employed in several studies of rotational energy transfer in  $\text{H}_2\text{-H}_2$  collisions within the rigid-rotor approximation at thermal energies [20, 24, 25, 26, 27, 28, 29] and also at ultralow energies [24, 25, 27]. Several full-dimensional potential surfaces have also been reported for the  $\text{H}_4$  system in recent years. They include the PESs of Schwenke [30], Aguado, Suárez and Paniagua (ASP) [31], Boothroyd, Martin, Keogh and Peterson (BMKP) [32], and the more recent work of Hinde [33]. These PESs have been adopted in a number of quantum scattering calculations of  $\text{H}_2\text{-H}_2$  that go beyond the rigid rotor approximation [34, 35, 36, 37, 38]. The BMKP and Schwenke PESs were recently employed in full-dimensional quantum calculations by Pogrebyna et al. [39, 40]. They reported the first quantum calculation of vibrational relaxation in collisions between  $\text{H}_2(v = 1, j = 0)$  and  $\text{H}_2(v = 0, j = 0)$  molecules using a time-independent quantum mechanical (TIQM) method within an angular momentum decoupling approximation called the coupled-states approximation (CSA). Lin et al. [41] used a time-dependent wave packet (TDWP) method and the CSA method to study pure rotational transitions in  $\text{H}_2(v = 0, j = 0) + \text{H}_2(v = 0, j = 0)$  collisions at thermal energies. Full-dimensional quantum studies without CSA have also been recently reported using the TDWP methods [42, 43, 44]. Gatti et al. [42] and Otto et al. [43] investigated para-para collisions involving  $\text{H}_2(v = 0, j = 0) + \text{H}_2(v = 0, j = 0)$ , and Panda et al. [44] reported ortho-para collisions of  $\text{H}_2(v = 1, 0, j = 1) + \text{H}_2(v = 0, 1, j = 0)$ . In a recent Communication [45], we reported rotational and vibrational relaxation of  $\text{H}_2(v = 1, j = 0, 2)$  in collisions with  $\text{H}_2(v = 0, j = 0, 2)$  at ultralow energies using the BMKP surface and a TIQM method that does not involve any angular momentum decoupling approximation. The calculations showed that indistinguishable molecule - molecule collisions may involve highly efficient near-resonant energy transfer if they are accompanied by simultaneous conservation of the total rotational angular momentum and internal energy of the molecules. This

mechanism was found to be independent of the initial vibrational excitation of the molecules.

In this article, we present the full quantum dynamics of rovibrational energy transfer in para-H<sub>2</sub> + para-H<sub>2</sub> system from ultralow to high collision energies and compare our results with previous quantum calculations [24, 27, 39, 43] and available experimental results [26, 46, 47]. We employ the BMKP PES and the full-dimensional TwoBC - quantum scattering program developed by Krems [48] implemented in our previous study [45]. The paper is organized as follows: In section II, we give an overview of the TIQM scattering theory of two <sup>1</sup>Σ diatomic molecules. In section III, we present state-to-state and initial state-selected cross sections and rate coefficients for the H<sub>2</sub>(*v* = 1, *j* = 0) + H<sub>2</sub>(*v* = 0, *j* = 0) and H<sub>2</sub>(*v* = 0, *j* = 0) + H<sub>2</sub>(*v* = 0, *j* = 0) collisions. Conclusions are given in section IV.

## II. MOLECULE - MOLECULE SCATTERING THEORY

The TIQM formalism for scattering of two <sup>1</sup>Σ diatomic molecules has been described by Takayanagi [49], Green [50], Alexander and DePristo [51], and Zarur and Rabitz [20], using the close-coupling (CC) formalism of Arthurs and Dalgarno [52]. A brief account of the theoretical formalism with particular emphasis on distinguishable versus indistinguishable molecule collisions is given here. For more details we refer to the original papers.

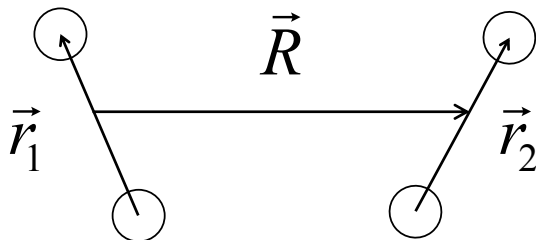


FIG. 1: Jacobi vectors used to describe molecule - molecule collisions.

Figure 1 shows the Jacobi vectors employed in the calculations where  $\vec{r}_1(r_1, \hat{r}_1)$  and  $\vec{r}_2(r_2, \hat{r}_2)$  describe the vectors joining the two atoms of the two H<sub>2</sub> molecules and  $\vec{R}(R, \hat{R})$  denote the vector joining the centers of mass of the two molecules. The Hamiltonian of the system,

$$H(\vec{r}_1, \vec{r}_2, \vec{R}) = T(\vec{r}_1) + T(\vec{r}_2) + T(\vec{R}) + V(\vec{r}_1, \vec{r}_2, \vec{R}), \quad (1)$$

is composed of a radial kinetic energy term  $T(\vec{R})$  describing the center-of-mass motion, two kinetic energy terms

$T(\vec{r}_1)$  and  $T(\vec{r}_2)$  for each diatomic molecule and the PES function,

$$V(\vec{r}_1, \vec{r}_2, \vec{R}) = U(\vec{r}_1, \vec{r}_2, \vec{R}) + V(\vec{r}_1) + V(\vec{r}_2), \quad (2)$$

describing the interactions between the four atoms. The terms  $V(\vec{r}_1)$  and  $V(\vec{r}_2)$  in Eq. (2) are the interaction energy potentials of the two H<sub>2</sub> molecules and  $U(\vec{r}_1, \vec{r}_2, \vec{R})$  is the interaction energy potential between the two molecules, which vanishes at large molecule - molecule separations,

$$\lim_{R \rightarrow \infty} U(\vec{r}_1, \vec{r}_2, \vec{R}) \rightarrow 0. \quad (3)$$

The angular dependence of the interaction potential may be expanded as

$$U(\vec{r}_1, \vec{r}_2, \vec{R}) = \sum_{\lambda} A_{\lambda}(r_1, r_2, R) Y_{\lambda}(\hat{r}_1, \hat{r}_2, \hat{R}), \quad (4)$$

with

$$Y_{\lambda}(\hat{r}_1, \hat{r}_2, \hat{R}) = \sum_{m_{\lambda}} \langle \lambda_1 m_{\lambda_1} \lambda_2 m_{\lambda_2} | \lambda_{12} m_{\lambda_{12}} \rangle Y_{\lambda_1 m_{\lambda_1}}(\hat{r}_1) Y_{\lambda_2 m_{\lambda_2}}(\hat{r}_2) Y_{\lambda_{12} m_{\lambda_{12}}}^*(\hat{R}), \quad (5)$$

where  $\lambda \equiv \lambda_1 \lambda_2 \lambda_{12}$  and  $m_{\lambda} \equiv m_{\lambda_1} m_{\lambda_2} m_{\lambda_{12}}$ . The notation  $\langle \lambda_1 m_{\lambda_1} \lambda_2 m_{\lambda_2} | \lambda_{12} m_{\lambda_{12}} \rangle$  represents a Clebsch-Gordan coefficient. Because the Hamiltonian defined in Eq. (1) is invariant under a rotation in space, the total angular momentum  $\vec{J}$  and its projection  $J_z$  on a space-fixed axis are conserved during the collision. In the following, we will discuss the close-coupling equations for both distinguishable and indistinguishable molecule - molecule collisions.

For collisions between two distinguishable molecules, the diabatic functions,

$$\phi_{vjl}^{JM\epsilon_I}(\vec{r}_1, \vec{r}_2, \hat{R}) = \chi_{v_j j_2}(r_1, r_2) \langle \hat{r}_1 \hat{r}_2 \hat{R} | j l J M \rangle, \quad (6)$$

serve as basis functions to expand the total wave function,

$$\Psi(\vec{r}_1, \vec{r}_2, \vec{R}) = \frac{1}{R} \sum_{v, j, l, J, M} F_{vjl}^{JM\epsilon_I}(R) \phi_{vjl}^{JM\epsilon_I}(\vec{r}_1, \vec{r}_2, \hat{R}), \quad (7)$$

where  $v \equiv v_1 v_2$  denotes the vibrational quantum numbers and  $j \equiv j_1 j_2 j_{12}$  denotes the rotational quantum numbers of the molecules. The function  $\chi_{v_j j_2}(r_1, r_2) = \chi_{v_1 j_1}(r_1) \chi_{v_2 j_2}(r_2)$  is the product of the vibrational wave functions of the two diatomic fragments and the angular function,

$$\langle \hat{r}_1 \hat{r}_2 \hat{R} | j l J M \rangle = \sum_{m_{j_1}, m_{j_2}, m_{j_{12}}, m_l} \langle j_1 m_{j_1} j_2 m_{j_2} | j_{12} m_{j_{12}} \rangle \langle j_{12} m_{j_{12}} l m_l | J M \rangle Y_{j_1 m_{j_1}}(\hat{r}_1) Y_{j_2 m_{j_2}}(\hat{r}_2) Y_{l m_l}(\hat{R}), \quad (8)$$

denotes the rotational wave function of the two molecules in the total angular momentum representation. In this representation, the rotational angular momenta  $\vec{j}_1$  and  $\vec{j}_2$  are coupled to give the total rotational momentum  $\vec{j}_{12}$  which is subsequently coupled to the orbital angular momentum  $\vec{l}$  to yield the total angular momentum  $\vec{J}$ . Under spatial inversion  $I$ , the basis functions (6) obey the eigenvalue equation,

$$I\phi_{vjl}^{JM\varepsilon_I} = \varepsilon_I\phi_{vjl}^{JM\varepsilon_I}, \quad (9)$$

with  $\varepsilon_I = (-1)^{j_1+j_2+l} = \pm 1$ . Substitution of Eq. (1) and Eq. (7) in the time-independent Schrödinger equation  $H\Psi = E\Psi$  leads to a set of close-coupling equations in the radial coordinate,  $R$ . The coupled equations become

$$\left\{ -\frac{\hbar^2}{2\mu} \frac{d^2}{dR^2} + \frac{\hbar^2 l(l+1)}{2\mu R^2} + \varepsilon_{vj} - E \right\} F_{vjl}^{JM\varepsilon_I}(R) + \sum_{v'j'l'} \mathcal{U}_{vjl,v'j'l'}^{JM\varepsilon_I}(R) F_{v'j'l'}^{JM\varepsilon_I}(R) = 0, \quad (10)$$

where  $\mu$  is the reduced mass of the molecule - molecule system. The total energy is  $E = \varepsilon_{vj} + E_c$  where  $\varepsilon_{vj} = \varepsilon_{v_1j_1} + \varepsilon_{v_2j_2}$  is the rovibrational energy of the two separated molecular fragments and  $E_c$  is the collision energy. The interaction potential matrix is given by

$$\mathcal{U}_{vjl,v'j'l'}^{JM\varepsilon_I}(R) = \sum_{\lambda} B_{v_{j_1j_2},v'_{j'_1j'_2}}^{\lambda}(R) f_{j_l,j'l'}^{J;\lambda}. \quad (11)$$

The radial interaction potential term  $B_{v_{j_1j_2},v'_{j'_1j'_2}}^{\lambda}(R)$  is given by

$$B_{v_{j_1j_2},v'_{j'_1j'_2}}^{\lambda}(R) = \int_0^{\infty} \int_0^{\infty} \chi_{v_{j_1j_2}}(r_1, r_2) A_{\lambda}(r_1, r_2, R) \chi_{v'_{j'_1j'_2}}(r_1, r_2) dr_1 dr_2, \quad (12)$$

and the function  $f_{j_l,j'l'}^{J;\lambda}$  is given in terms of  $3-j$ ,  $6-j$ , and  $9-j$  symbols by

$$f_{j_l,j'l'}^{J;\lambda} = (4\pi)^{-3/2} (-1)^{j_1+j_2+j'_{12}+J} [\lambda, j, l, j', l', \lambda_{12}]^{1/2} \begin{pmatrix} j_1 & j'_1 & \lambda_1 \\ 0 & 0 & 0 \end{pmatrix} \begin{pmatrix} j_2 & j'_2 & \lambda_2 \\ 0 & 0 & 0 \end{pmatrix} \begin{pmatrix} l & l' & \lambda_{12} \\ 0 & 0 & 0 \end{pmatrix} \left\{ \begin{matrix} l & l' & \lambda_{12} \\ j'_{12} & j_{12} & J \end{matrix} \right\} \left\{ \begin{matrix} j'_{12} & j'_2 & j'_1 \\ j_{12} & j_2 & j_1 \\ \lambda_{12} & \lambda_2 & \lambda_1 \end{matrix} \right\}, \quad (13)$$

with the notation

$$[x_1, x_2, \dots, x_n] = (2x_1 + 1)(2x_2 + 1) \dots (2x_n + 1). \quad (14)$$

For two indistinguishable molecules, one has to symmetrize the wave function with respect to the exchange-permutation symmetry of the molecules. Under molecule permutation  $P$ ,  $P\phi_{vjl}^{JM\varepsilon_I} = (-1)^{j_1+j_2+j_{12}+l} \phi_{vjl}^{JM\varepsilon_I}$ , where

$\bar{v} \equiv v_2v_1$  and  $\bar{j} \equiv j_2j_1j_{12}$ . As a consequence, properly symmetrized exchange-permutation invariant states must be employed for the basis set,

$$\phi_{vjl}^{JM\varepsilon_I\varepsilon_P}(\vec{r}_1, \vec{r}_2, \hat{R}) = \Delta_{v_{j_1j_2}} \left[ \phi_{vjl}^{JM\varepsilon_I} + \varepsilon_P (-1)^{j_1+j_2+j_{12}+l} \phi_{\bar{v}\bar{j}l}^{JM\varepsilon_I} \right], \quad (15)$$

with  $\varepsilon_P = \pm 1$ ,  $\Delta_{v_{j_1j_2}} = [2(1 + \delta_{v_1v_2} \delta_{j_1j_2})]^{-1/2}$ , and

$$P\phi_{vjl}^{JM\varepsilon_I\varepsilon_P} = \varepsilon_P \phi_{vjl}^{JM\varepsilon_I\varepsilon_P}. \quad (16)$$

The total wavefunction is expanded as

$$\Psi(\vec{r}_1, \vec{r}_2, \vec{R}) = \frac{1}{R} \sum_{v,j,l,J,M}^* F_{vjl}^{JM\varepsilon_I\varepsilon_P}(R) \phi_{vjl}^{JM\varepsilon_I\varepsilon_P}(\vec{r}_1, \vec{r}_2, \hat{R}), \quad (17)$$

where the superscript over the sum symbol indicates a summation over states that have to follow a ‘‘well ordered’’ classification as discussed in Ref. [49, 50, 51]. We choose  $v_1 > v_2$  or when  $v_1 = v_2$ ,  $j_1 \geq j_2$ . The time-independent Schrödinger equation yields a set of close-coupling equations,

$$\left\{ -\frac{\hbar^2}{2\mu} \frac{d^2}{dR^2} + \frac{\hbar^2 l(l+1)}{2\mu R^2} + \varepsilon_{vj} - E \right\} F_{vjl}^{JM\varepsilon_I\varepsilon_P}(R) + \sum_{v'j'l'}^* \mathcal{U}_{vjl,v'j'l'}^{JM\varepsilon_I\varepsilon_P}(R) F_{v'j'l'}^{JM\varepsilon_I\varepsilon_P}(R) = 0, \quad (18)$$

with the interaction potential matrix,

$$\mathcal{U}_{vjl,v'j'l'}^{JM\varepsilon_I\varepsilon_P}(R) = 2\Delta_{v_{j_1j_2}} \Delta_{v'_{j'_1j'_2}} [\mathcal{U}_{vjl,v'j'l'}^{JM\varepsilon_I} + \varepsilon_P (-1)^{j'_1+j'_2+j'_{12}+l} \mathcal{U}_{v_{j_1j_2},v'_{j'_1j'_2}}^{JM\varepsilon_I}(R)]. \quad (19)$$

Because of the indistinguishability of the molecules and the summation over the ‘‘well ordered’’ states, the size of the set of close-coupling equations (18) is smaller than the set (10).

The close-coupling equations (10) or (18) are solved for each value of  $R$  using the log-derivative matrix propagation method of Johnson [53] and Manolopoulos [54]. The log-derivative matrix is propagated to a matching distance where asymptotic boundary conditions are applied to obtain the scattering matrix,  $S$ , for given values of  $J$ ,  $\varepsilon_I$  and  $\varepsilon_P$ . For distinguishable molecule collisions, the state-to-state cross section is given by

$$\sigma_{v_1j_1v_2j_2 \rightarrow v'_1j'_1v'_2j'_2}(E_c) = \frac{\pi}{(2j_1 + 1)(2j_2 + 1)k^2} \sum_{j_{12}j'_{12}ll'J\varepsilon_I} (2J + 1) |\delta_{vjl,v'j'l'} - S_{vjl,v'j'l'}^{J\varepsilon_I}(E_c)|^2, \quad (20)$$

where the wave vector  $k^2 = 2\mu E_c/\hbar^2$ . For indistinguishable molecules, the state-to-state cross section is given by

a statistically weighted sum of the exchange-permutation symmetrized cross sections,

$$\sigma_{v_1 j_1 v_2 j_2 \rightarrow v'_1 j'_1 v'_2 j'_2}(E_c) = W^+ \sigma^{\varepsilon_P=+1} + W^- \sigma^{\varepsilon_P=-1}, \quad (21)$$

where

$$\sigma^{\varepsilon_P} = \frac{\pi(1 + \delta_{v_1 v_2} \delta_{j_1 j_2})(1 + \delta_{v'_1 v'_2} \delta_{j'_1 j'_2})}{(2j_1 + 1)(2j_2 + 1)k^2} \sum_{j_{12} j'_{12} l' J \varepsilon_I}^* (2J + 1) |\delta_{v_{jl}, v'_{j'l'}} - S_{v_{jl}, v'_{j'l'}}^{J \varepsilon_I \varepsilon_P}(E_c)|^2. \quad (22)$$

For collisions between para-H<sub>2</sub> molecules (nuclear spin  $I = 0$ ),  $W^+ = 1, W^- = 0$  so that only the  $\varepsilon_P = +1$  exchange-permutation symmetry is needed in the close-coupling calculations, while for collisions between ortho-H<sub>2</sub> molecules (nuclear spin  $I = 1$ ),  $W^+ = 2/3, W^- = 1/3$  and both exchange-permutation symmetries  $\varepsilon_P = \pm 1$  are needed. The total inelastic cross section is the sum of all inelastic state-to-state cross sections. The state-to-state rate coefficients are obtained by integrating the corresponding cross sections over the Maxwell-Boltzmann distribution of velocities,

$$k_{v_1 j_1 v_2 j_2 \rightarrow v'_1 j'_1 v'_2 j'_2}(T) = \frac{1}{k_B T} \left( \frac{8}{\pi \mu k_B T} \right)^{1/2} \int_0^\infty \sigma_{v_1 j_1 v_2 j_2 \rightarrow v'_1 j'_1 v'_2 j'_2}(E_c) e^{-E_c/(k_B T)} E_c dE_c. \quad (23)$$

### III. RESULTS AND DISCUSSION

#### A. Computational details

In this study we investigate the scattering of two identical para-H<sub>2</sub> molecules using the BMKP PES [32]. For identical molecule collisions, the rovibrational quantum numbers obey the “well ordered states” classification [49, 50, 51]. For convenience we use the term “combined molecular state” (CMS), for a combination of two

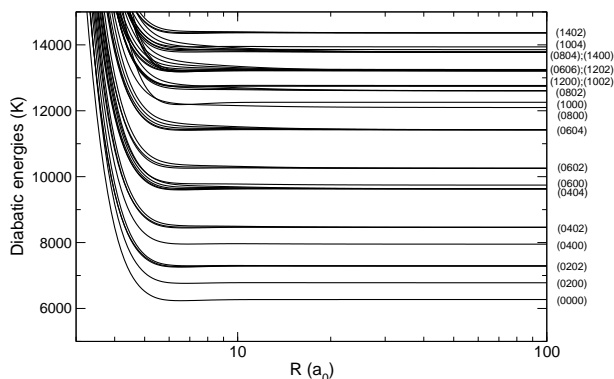


FIG. 2: The effective potentials,  $V_{\text{eff}}^J$ , as functions of  $R$  for the H<sub>4</sub> system for  $J = 0, \varepsilon_I = +1, \varepsilon_P = +1$ .

rovibrational states of two H<sub>2</sub> molecules. In this notation, H<sub>2</sub>( $v_1, j_1$ ) + H<sub>2</sub>( $v_2, j_2$ ) collisions will be denoted as ( $v_1 j_1 v_2 j_2$ ) and its energy is given by  $\varepsilon_{vj} = \varepsilon_{v_1 j_1} + \varepsilon_{v_2 j_2}$ . The CMS represents a unique quantum state of the diatom - diatom system before or after the collision. To gain physical insights into the scattering process and also to roughly estimate the number of CMSs to be included in the scattering calculations, we plot in Fig. 2 the effective potentials which are composed of the diabatic energies and the centrifugal terms,

$$V_{\text{eff}}^J(R) = \varepsilon_{vj} + \mathcal{U}_{v_{jl}, v'_{j'l'}}^{JM \varepsilon_I \varepsilon_P}(R) + \frac{\hbar^2 l(l+1)}{2\mu R^2}, \quad (24)$$

as functions of the radial coordinate,  $R$ , evaluated using the BMKP PES. At large separations, the energies of the different potential curves converge to that of the corresponding CMSs as indicated by the numbers ( $v_1 j_1 v_2 j_2$ ) in Fig. 2. The energy of the CMS (0000) is 6270.73 K and that of (0200) is 6780.35 K. For the vibrationally excited case, (1000), the energy is 12257.57 K. The energy is relative to the minimum of the H<sub>2</sub> potential. Since the interaction potential between two H<sub>2</sub> molecules is relatively weak the density of CMSs is rather sparse. The number of diabatic channels included in the calculation depends on the energy. For collision energies  $E_c < 100$  K, a cut-off energy is used to restrict the number of channels. This allows one to include all rotational and vibrational levels below the cut-off energy in the scattering calculations. We used cut-off energies of 20142.76 K (14000 cm<sup>-1</sup>) for  $J = 0 - 3$ , and 15826.45 K (11000 cm<sup>-1</sup>) for  $J = 4 - 10$  for ultralow energy calculations. However, this approach may lead to a proliferation in the number of channels at higher energies as the cut-off energy needs to be higher. Thus only a restricted set of rovibrational levels are included in the calculations. In the present work we retained all CMSs with quantum numbers  $v = 0, j = 0 - 8$ , and  $v = 1, j = 0, 2$  for calculations at higher energies. The close-coupling equations (18) were propagated using the log-derivative matrix propagation method of Johnson [53] and Manolopoulos [54] to an asymptotic matching distance of  $R = 53 a_0$ . For all collision energies, the inelastic cross section is converged at this value of the matching distance. However, to get converged elastic cross section for ultralow energies  $E_c < 1$  K, we propagate the elastic channel from  $R = 53 a_0$  to a sufficiently large distance, at which the interaction potential  $U$  in Eq. (2) is less than  $10^{-5} \times E_c$ .

#### B. Vibrational relaxation in H<sub>2</sub>( $v = 1, j = 0$ ) + H<sub>2</sub>( $v = 0, j = 0$ ) collisions

In the upper panel of Fig. 3 we show the  $J$ -resolved partial cross sections and their sum for the elastic channel for collision energies ranging from  $10^{-3} - 120$  K. Though only the  $s$ -wave contributes at energies below  $10^{-2}$  K, the partial wave sum requires up to  $J = 10$  at  $E_c = 100$  K to

yield converged cross sections. The state-to-state inelastic cross sections and their sum are shown in the lower panel of Fig. 3 for  $\text{H}_2(v=1, j=0) + \text{H}_2(v=0, j=0)$  collisions for  $E_c = 10^{-3} - 120$  K. The cross sections of the inelastic processes are much smaller than that of elastic scattering. Due to the small anisotropy of the interaction potential with respect to the stretching of the molecule, the interaction potential matrix elements responsible for vibrational relaxation channels are quite small compared to the isotropic part responsible for elastic scattering. Thus, the couplings between different CMSs are rather weak and state-to-state transitions are less probable than elastic scattering. The diabatic potential curves in Fig. 2 shows that the density of states is quite small and the energy levels are sparsely spaced leading to small inelastic couplings. This is in contrast with the heavier alkali-metal systems with very high density of states, for which elastic scattering is less important than inelastic collisions at ultralow collision energies [18]. In Fig. 3, the CMS (0800) is the most probable final state. This corresponds to a case where the vibrationally excited molecule  $\text{H}_2(v=1, j=0)$  relaxes to the rotationally excited  $\text{H}_2(v=0, j=8)$  state upon collisions with the ground state molecule  $\text{H}_2(v=0, j=0)$ . The final state distribution is determined by a compromise between conservation of the total internal energy and the rotational angular momenta of the colliding molecules.

In Fig. 4 we present the state-to-state rovibrational populations of the two molecules in  $\text{H}_2(v=1, j=0) + \text{H}_2(v=0, j=0)$  collisions at an energy of  $E_c = 10^{-3}$  K. Since rotational level resolved state-to-state cross sections are more difficult to converge compared to initial state-selected cross sections, we also include results from our convergence studies. Figure 4 shows that the results are robust and converged with respect to all numerical parameters employed in the calculations. The upper panel shows cross sections for different values of  $\lambda_1 = \lambda_2$  in Eq. (4). It is seen that  $\lambda_1 = \lambda_2 = 8$  or higher is needed to accurately calculate cross sections for the dominant final CMS, (0800). The convergence of the results with respect to the cut-off energy, the size  $\Delta R$  of the radial interval, the number of DVR points  $N_{r_1} = N_{r_2} \equiv N_r, N_{\theta_1} = N_{\theta_2} \equiv N_\theta$ , and  $N_\phi$  used for the vibrational and rotational wave functions are presented in the lower panel. These results are obtained with  $\lambda_1 = \lambda_2 = 8$  for the angular expansion of the interaction potential. For the results reported in the final production calculations for the BMKP PES we used  $\lambda_1 = \lambda_2 = 8, \Delta R = 0.05 a_0, N_\theta = 14, N_\phi = 8$ , and  $N_r = 24$ .

Figure 4 shows that vibrational relaxation of  $\text{H}_2(v=1, j=0)$  by collisions with  $\text{H}_2(v=0, j=0)$  is driven by high order anisotropic terms of the BMKP PES. Pogrebnya et al. [39] had previously investigated this issue and they had found that the high anisotropic terms of the BMKP PES lead to large values of the vibrational relaxation rate coefficients compared to experimental results. They found that a restricted version of this PES, referred to as the BMKPE PES which includes only

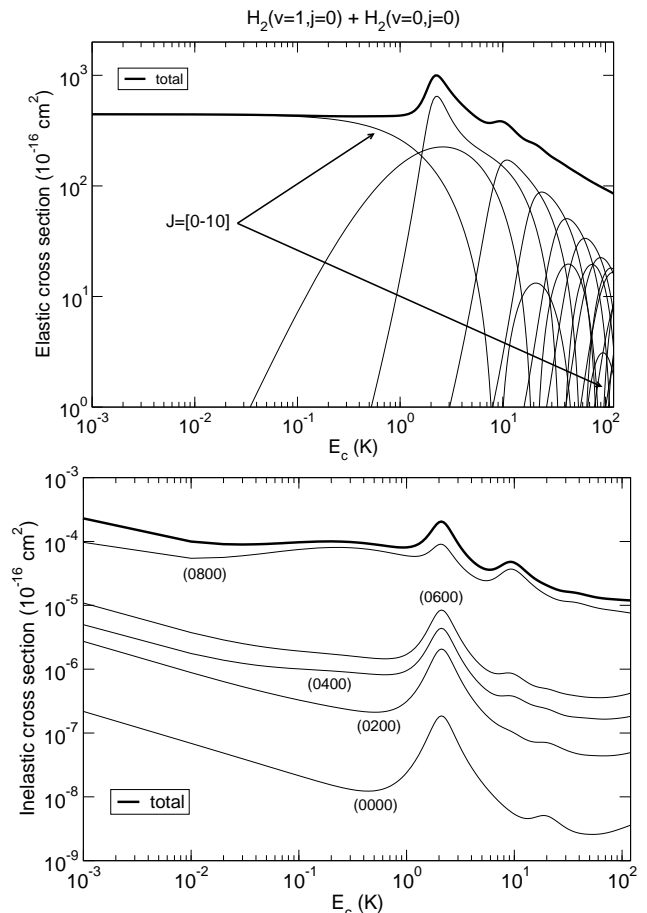


FIG. 3: Upper panel: Partial-wave resolved and total elastic cross sections for  $\text{H}_2(v=1, j=0) + \text{H}_2(v=0, j=0)$  collisions as a function of the collision energy. Lower panel: Inelastic state-to-state cross sections for the  $\text{H}_2(v=1, j=0) + \text{H}_2(v=0, j=0)$  system as a function of the collision energy. For clarity, only the final CMSs (0j00) have been shown.

$\lambda_1 = \lambda_2 = 2$  components in Eq. (4) for the angular expansion of the interaction potential, yields better results in comparison with experimental data. In the upper panel of Fig. 5 we show the cross section for  $\text{H}_2(v=1, j=0) + \text{H}_2(v=0, j=0) \rightarrow \text{H}_2(v=0) + \text{H}_2(v=0)$  collisions for  $E_c = 0.001 - 1$  eV evaluated using the BMKPE (filled squares) and BMKP (filled circles) PESs. The corresponding results of Pogrebnya et al. [39] are also shown (open squares and circles) for comparison. While the results on the BMKPE PES are in overall good agreement, the results on the BMKP PES differ significantly at low collision energies (0.001 eV). The agreement improves with increase in collision energy and both cross sections show similar energy dependence for  $E_c = 0.1 - 1$  eV. In the lower panel of Fig. 5, we compare state-to-state cross sections at  $E_c = 0.01$  eV for the BMKPE (white) and BMKP (black) PESs with the corresponding results of Pogrebnya et al. (dashed or gray). Our results on both

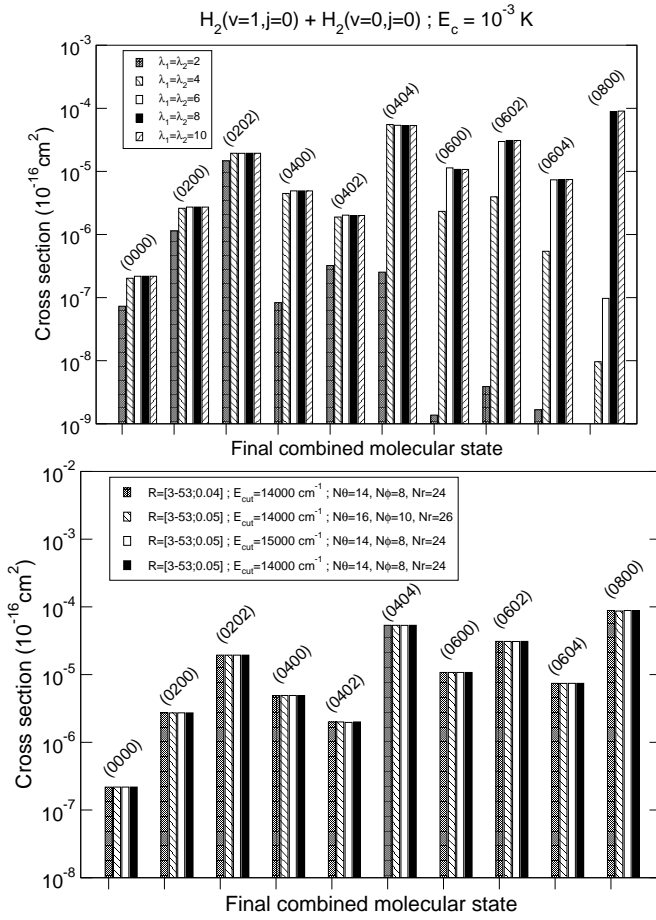


FIG. 4: State-to-state cross sections for  $\text{H}_2(v=1, j=0) + \text{H}_2(v=0, j=0)$  collisions at an energy of  $10^{-3}$  K. The parameters corresponding to the black distributions are adopted in the final production calculations. Upper panel: convergence with respect to the angular anisotropic terms of the PES. Lower panel: convergence with respect to the number of points for the radial and angular integrations and the cut-off energy for the basis set.

PESs are in good agreement with those of Pogrebnya et al. for the CMSs (0000), (0200), (0202), (0400), (0402) but differ for the CMSs (0404), (0600), (0602), (0604), (0800). We believe that the differences are due to the CSA method employed in the work of Pogrebnya et al. This applies to the results in both panels of Fig. 5. The maximum value of the total angular momentum projection quantum number,  $\Omega$ , on the body-fixed axis  $\vec{R}$  used in the calculations of Pogrebnya et al. is  $|\Omega|_{\max} = 4$ . In a body-fixed frame, the orbital angular momentum  $\vec{l}$  is always perpendicular to the body-fixed axis  $\vec{R}$  and the value  $m_l$  of its projection on  $\vec{R}$  is zero. This implies that the projection of  $\vec{J} = \vec{j}_{12} + \vec{l}$  on the body-fixed axis is  $\Omega = m_{j_{12}}$ . If  $|\Omega|_{\max}$  is restricted to 4, so does  $|m_{j_{12}}|$ . This is equivalent to exclude all projection quantum numbers  $|m_{j_{12}}| > 4$ . Since no such restriction is imposed in our calculations, the differences between the exact and

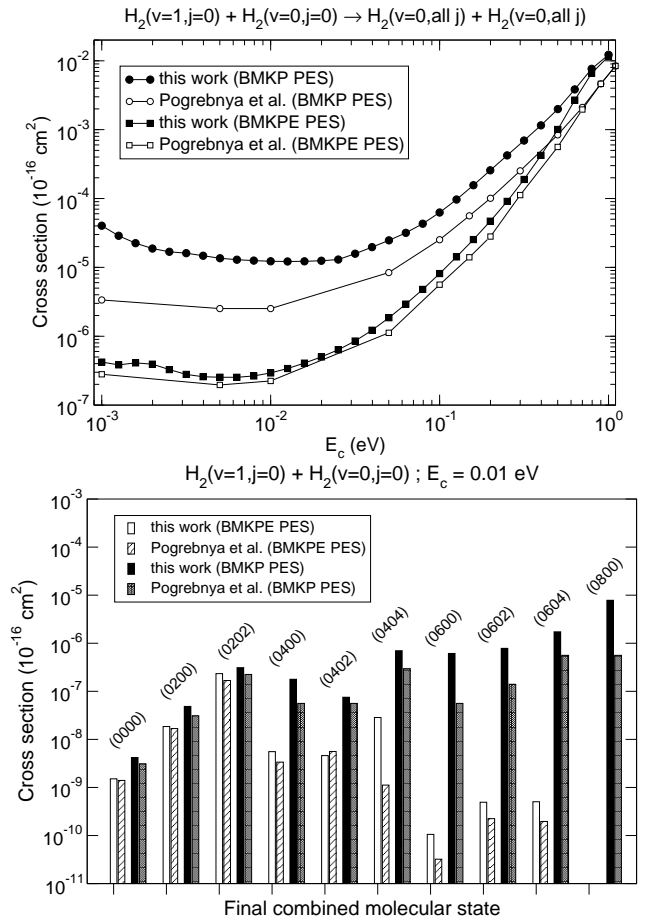


FIG. 5: Upper panel: Vibrational relaxation cross sections as functions of the collision energy for the  $\text{H}_2(v=1, j=0) + \text{H}_2(v=0, j=0)$  system. Lower panel: State-to-state cross sections at a collision energy of  $E_c = 0.01$  eV.

CSA methods for CMSs with quantum numbers  $j_{12} > 4$  and  $|m_{j_{12}}| > 4$ , such as (0404), (0600), (0602), (0604), (0800), are attributed to the restriction on  $\Omega$  imposed in the CSA calculations. The good agreement between the full quantum and CSA methods for the BMKPE PES is attributed to the negligible contributions of the final states (0404), (0600), (0602), (0604) and (0800). Since the restriction on  $\Omega$  primarily impacts these final states, it does not significantly affect the cross sections computed using the BMKPE PES.

The rate coefficients for the vibrational relaxation of  $\text{H}_2(v=1, j=0)$  in collision with  $\text{H}_2(v=0, j=0)$  as functions of the temperature are reported in Fig. 6 for the BMKP PES (solid curve) and the BMKPE PES (dashed curve). The experimental results of Audibert et al. [46] are also shown for comparison. For the reasons discussed above, the BMKP PES predicts rate coefficients that are about two orders of magnitude larger than the experimental results for  $T < 200$  K. The less anisotropic BMKPE PES yields results in better agreement with the experimental results. The agreement is

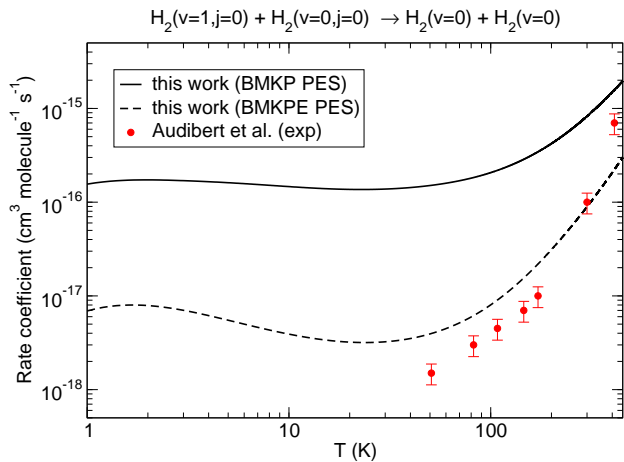


FIG. 6: (Color online) Rate coefficient for the vibrational relaxation of  $\text{H}_2(v=1, j=0)$  in collisions with  $\text{H}_2(v=0, j=0)$  as a function of the temperature. Results obtained using the BMKP and BMKPE PESs are compared with the experimental results of Audibert et al. [46].

very good at  $T = 300$  K. At lower temperatures, the calculations predict slightly larger values than the experimental results. For  $T > 300$  K, the experimental result is higher than the theoretical results on the BMKPE PES.

### C. Rotational excitation and de-excitation in $\text{H}_2(v=0, j=0, 2) + \text{H}_2(v=0, j=0, 2)$ collisions

In Fig. 7 we show cross sections for  $\text{H}_2(v=0, j=0) + \text{H}_2(v=0, j=0)$  (upper panel),  $\text{H}_2(v=0, j=2) + \text{H}_2(v=0, j=0)$  (middle panel) and  $\text{H}_2(v=0, j=2) + \text{H}_2(v=0, j=2)$  (lower panel) collisions on the BMKP PES. Previous results of Lee et al. [27] on the BMKP and DJ PESs and Forrey [24] on the ZR PES based on the rigid rotor model are also shown for comparison. The results on the BMKP PES in the upper panel show that the rigid rotor approximation is reliable in predicting elastic cross sections for collisions between two ground state  $\text{H}_2$  molecules. The DJ potential predicts similar results as the BMKP potential except for the slight shift in the location of the resonance at about  $E_c = 2$  K. The agreement between the DJ and BMKP results is excellent for collision energies above 4 K. Overall, the elastic cross section appears to be less sensitive to the choice of the PES and the dynamics approximation. In the middle panel of Fig. 7 we show the elastic and inelastic rotational de-excitation cross sections for  $\text{H}_2(v=0, j=2) + \text{H}_2(v=0, j=0)$  collisions. As in the case of collisions between ground state molecules, the elastic cross sections from rigid rotor calculations of Lee et al. [27] using the DJ PES and the present full-dimensional results on the BMKP surface are in good agreement with each other. However, the inelastic cross sections show significant differences. The inelastic rotational de-excitation

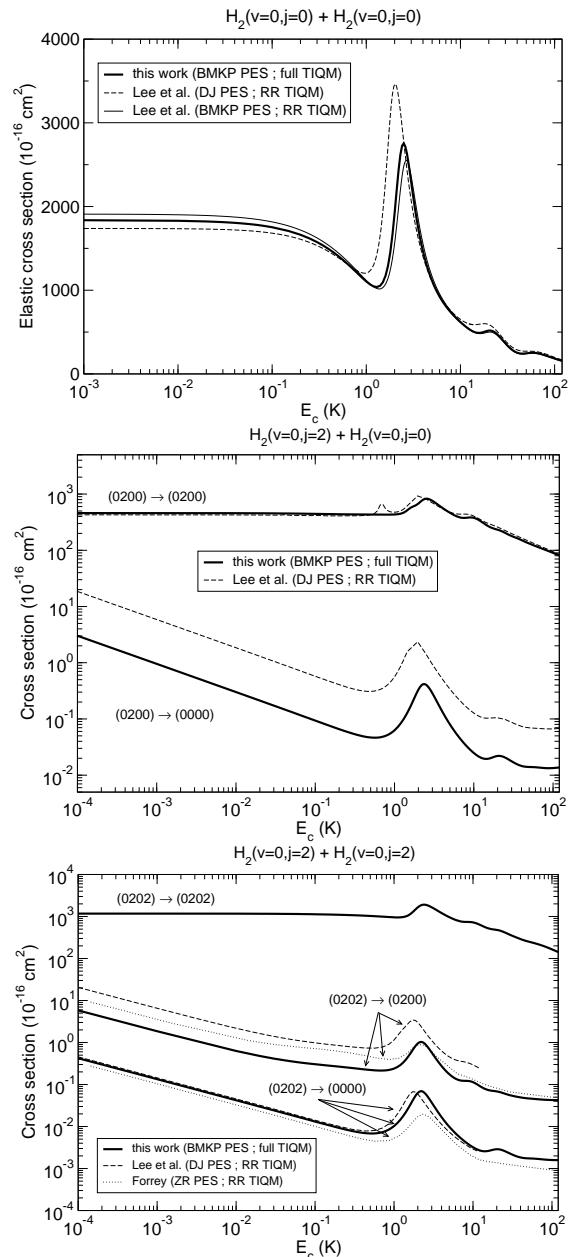


FIG. 7: Elastic and inelastic cross sections as functions of the collision energy. Upper panel: Elastic cross sections for  $\text{H}_2(v=0, j=0) + \text{H}_2(v=0, j=0)$  collisions. Middle panel: Elastic and inelastic cross sections for  $\text{H}_2(v=0, j=2) + \text{H}_2(v=0, j=0)$  collisions. Lower panel: Elastic and inelastic cross sections for  $\text{H}_2(v=0, j=2) + \text{H}_2(v=0, j=2)$  collisions.

cross section on the DJ PES is about an order of magnitude larger than that derived from the BMKP PES. This confirms conclusions derived from previous calculations [27, 43] that the BMKP PES is not reliable in predicting accurate values of rotational excitation cross sections, especially for the  $\Delta j = 2$  rotational transitions. In the lower panel we show elastic and inelastic rota-

tional de-excitation cross sections for  $\text{H}_2(v=0, j=2) + \text{H}_2(v=0, j=2)$  collisions. Interestingly,  $(0202) \rightarrow (0000)$  inelastic cross sections are comparable in magnitude for the BMKP PES, the DJ PES, and also for the ZR PES. However, for the  $(0202) \rightarrow (0200)$  transition, the BMKP potential yields smaller cross sections than DJ and ZR potentials for collision energies below 2 K. The agreement improves for higher collision energies, especially with that from the ZR potential.

The elastic cross section of the  $\text{H}_2(v=0, j=0) + \text{H}_2(v=0, j=0)$  collision is shown in Fig. 8 for collision energies up to 0.03 eV. The theoretical results of Lee et al. [27] and experimental results of Bauer et al. [47] are also included for comparison. The present results do not differ significantly from the results of Lee et al. The full calculation predicts slightly larger values for the elastic cross section compared to the rigid rotor results. Overall, the DJ PES predicts results in better agreement with the experimental results.

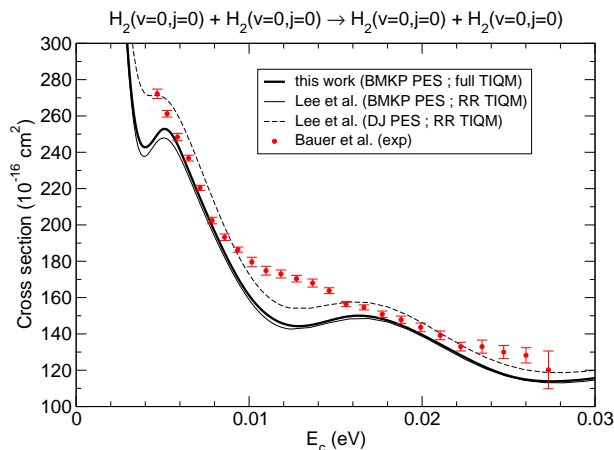


FIG. 8: (Color online) Elastic cross section for  $\text{H}_2(v=0, j=0) + \text{H}_2(v=0, j=0)$  collisions as a function of the incident collision energy. The experimental results of Bauer et al. [47] and theoretical results of Lee et al. [27] are also shown.

A number of recent studies have reported rotational excitation cross sections in collisions between two rovibrationally ground state  $\text{H}_2$  molecules [27, 42, 43]. The studies of Gatti et al. [42] and Otto et al. [43] employed the full-dimensional multiconfiguration time-dependent Hartree (MCTDH) approach while that of Lee et al. [27] employed the TIQM approach within the rigid rotor approximation. Though the agreement between these calculations were generally good, important differences were found for some transitions, especially for  $(0000) \rightarrow (0202)$  and  $(0000) \rightarrow (0404)$  transitions. In Fig. 9 we show rotational excitation cross sections in  $\text{H}_2(v=0, j=0) + \text{H}_2(v=0, j=0)$  collisions leading to final CMSs  $(0200)$ ,  $(0202)$ ,  $(0400)$ ,  $(0402)$ , and  $(0404)$ . To obtain converged cross sections, these calculations include contributions from  $J=0-100$ . Also included are TIQM rigid rotor results from the present work, and full-dimensional

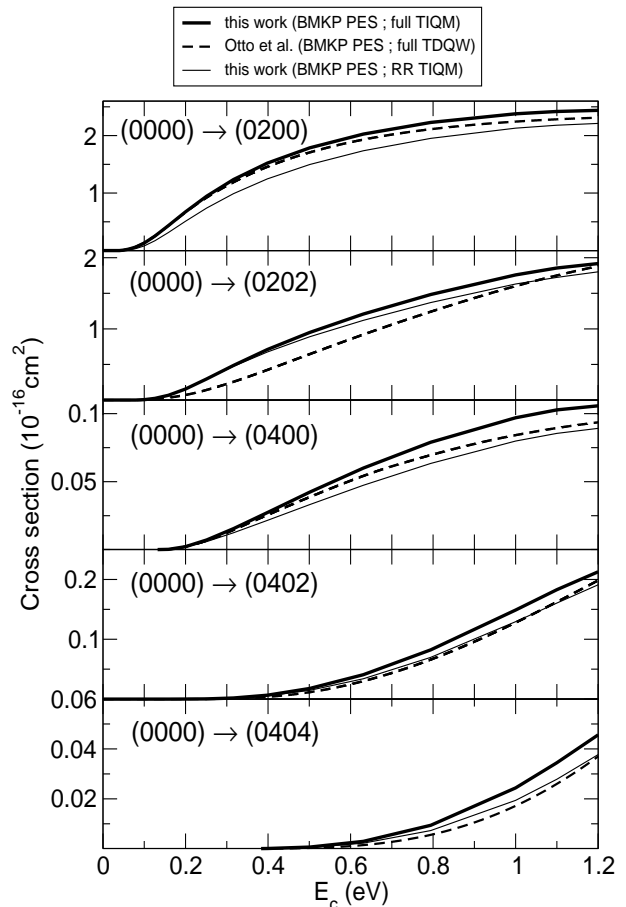


FIG. 9: State-to-state cross sections for rotational excitation in  $\text{H}_2(v=0, j=0) + \text{H}_2(v=0, j=0)$  collisions as functions of the collision energy. The results of Otto et al. [43] are included for comparison.

time-dependent calculations of Otto et al. [43]. Figure 4 of Ref. [43] presents similar comparison with the results of Lee et al. [27], Lin et al. [41], and Sultanov et al. [28]. Figure 9 shows that our results are generally in good agreement with those of Otto et al. for the  $(0000) \rightarrow (0200)$  and  $(0000) \rightarrow (0400)$  transitions. The agreement is better for collision energies lower than 0.5 eV. The rigid rotor calculations from the present study underestimate the cross sections. The largest discrepancy between the present work and the time-dependent calculations occur for the  $(0000) \rightarrow (0202)$  transition. Overall, for all of the transitions shown in Fig. 9 the agreement with the time-dependent results is better at low collision energies and it deteriorates with increasing collision energy. This also applies to the rigid rotor results compared to the full-dimensional calculations from the present study. Our full-dimensional calculations include  $v=0, j=0-8$  and  $v=1, j=0-2$  levels in the basis set. It is possible that a larger basis set with additional rotational levels would yield results in better agreement with the time-dependent results at higher energies. However, this does not explain



the discrepancy between the time-dependent and time-independent calculations for the (0000)  $\rightarrow$  (0202) transition. Calculations using significantly larger basis sets are computationally demanding and beyond the scope of this paper.

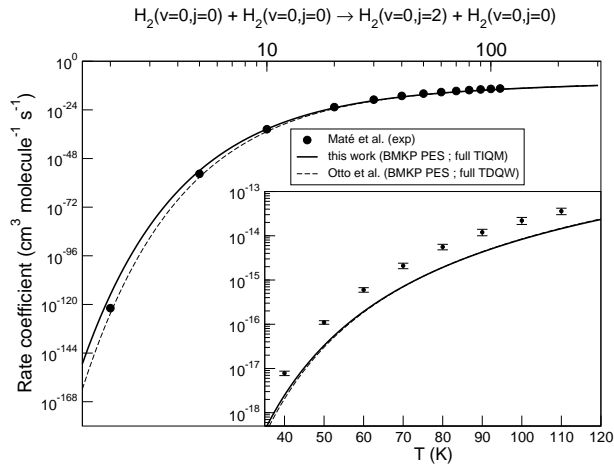


FIG. 10: Rate coefficient as a function of the temperature for  $\text{H}_2(v=0, j=0) + \text{H}_2(v=0, j=0) \rightarrow \text{H}_2(v=0, j=2) + \text{H}_2(v=0, j=0)$  collisions. The TDWP results of Otto et al. [43] and experimental results of Maté et al. [26] are also included for comparison. The TDWP results are almost identical to the present results for  $T > 10$  K.

In Fig. 10 we show the temperature dependence of the rate coefficient for  $\text{H}_2(v=0, j=0) + \text{H}_2(v=0, j=0) \rightarrow \text{H}_2(v=0, j=2) + \text{H}_2(v=0, j=0)$  collisions along with the corresponding experimental results of Maté et al. [26] and the TDQW results of Otto et al. [43]. It has previously been shown that for this transition the BMKP PES underestimates the rate coefficient by about an order of magnitude [27, 43]. Our results confirm this finding. As Fig. 10 illustrates, our results are in very good agreement with those of Otto et al. [43] although the corresponding cross sections given in Fig. 9 show some differences at collision energies above 0.5 eV. This is because in the temperature range of 10 – 300 K, the main contribution to the rate coefficients occurs from cross sections at energies below 0.5 eV.

#### IV. CONCLUSION

In this paper we present explicit quantum scattering calculations of collisions between two para- $\text{H}_2$  molecules

in  $v=0$  and  $v=1$  vibrational levels from ultralow to thermal energies. A new code [48] based on a full-dimensional time-independent quantum scattering method has been employed for the calculations. Using this code we have been able to test the reliability of the coupled-states approximation for accurately predicting vibrational relaxation rate coefficients for  $\text{H}_2(v=1, j=0) + \text{H}_2(v=0, j=0)$  collisions. Comparison of our results with previous coupled-states calculations of Pogrebnya and Clary shows that the coupled-states approximation is not very reliable for this system in predicting vibrational relaxation cross sections at low energies. This is in part due to the high order angular anisotropic terms of the  $\text{H}_4$  BMKP PES. We obtained good agreement with the results of Pogrebnya and Clary for the BMKPE potential which excludes the high order anisotropic terms of the interaction potential. The relaxation rate coefficient is found to be generally in good agreement with experimental results when the BMKPE PES is used.

We explored pure rotational transitions in  $\text{H}_2(v=0, j=0, 2) + \text{H}_2(v=0, j=0, 2)$  collisions at ultralow energies and compared our results with those of Forrey and Lee et al., using different PESs. While the inelastic processes are sensitive to the PES employed, the elastic processes do not show significant differences. We also presented pure rotational excitation of  $\text{H}_2(v=0, j=0, 2) + \text{H}_2(v=0, j=0, 2)$  and compared our results with those of Otto et al. The TIQM and TDWP methods give comparable results for collision energies up to 0.5 eV. But some discrepancies exist for (0000)  $\rightarrow$  (0202) and (0000)  $\rightarrow$  (0404) rotational transitions, presumably due to the contributions from the  $v=1$  level.

Future works will involve ortho-para and ortho-ortho collisions of hydrogen molecules as well as  $\text{H}_2$ -HD,  $\text{D}_2$ - $\text{D}_2$  and HD-HD collisions.

#### V. ACKNOWLEDGMENTS

This work was supported by NSF grants # PHY-0555565, ATM-0635715, AST-0607524, and NASA grant NNG06GC94G. We thank R. V. Krems for initial collaboration on this project and for many stimulating discussions and consultations. We thank T.-G. Lee and F. Otto for providing us their theoretical results.

- 
- [1] J. T. Bahns, W. Stwalley, and P. L. Gould, *Adv. At. Mol. Opt. Phys.* **42**, 171 (2000).  
 [2] F. Masnou-Seeuws and P. Pillet, *Adv. At. Mol. Opt. Phys.* **47**, 53 (2001).

- [3] H. L. Bethlem and G. Meijer, *Int. Rev. Phys. Chem.* **22**, 73 (2003).  
 [4] J. Doyle, B. Friedrich, R. V. Krems, and F. Masnou-Seeuws, *Eur. Phys. J. D* **31**, 149 (2004).

- [5] J. M. Hutson and P. Soldán, *Int. Rev. Phys. Chem.* **25**, 497 (2006).
- [6] J. M. Hutson and P. Soldán, *Int. Rev. Phys. Chem.* **26**, 1 (2007).
- [7] R. V. Krems, *Int. Rev. Phys. Chem.* **24**, 99 (2005).
- [8] R. V. Krems, *Phys. Chem. Chem. Phys.* **10**, 4079 (2008).
- [9] N. Balakrishnan and A. Dalgarno, *Chem. Phys. Lett.* **341**, 652 (2001).
- [10] P. F. Weck and N. Balakrishnan, *Int. Rev. Phys. Chem.* **25**, 283 (2006).
- [11] G. Quéméner and N. Balakrishnan, *J. Chem. Phys.* **128**, 224304 (2008).
- [12] E. Bodo and F. A. Gianturco, *Int. Rev. Phys. Chem.* **25**, 313 (2006).
- [13] P. Soldán, M. T. Cvitaš, J. M. Hutson, P. Honvault, and J.-M. Launay, *Phys. Rev. Lett.* **89**, 153201 (2002).
- [14] G. Quéméner, P. Honvault, and J.-M. Launay, *Eur. Phys. J. D* **30**, 201 (2004).
- [15] G. Quéméner, P. Honvault, J.-M. Launay, P. Soldán, D. E. Potter, and J. M. Hutson, *Phys. Rev. A* **71**, 032722 (2005).
- [16] M. T. Cvitaš, P. Soldán, J. M. Hutson, P. Honvault, and J.-M. Launay, *Phys. Rev. Lett.* **94**, 033201 (2005).
- [17] M. T. Cvitaš, P. Soldán, J. M. Hutson, P. Honvault, and J.-M. Launay, *Phys. Rev. Lett.* **94**, 200402 (2005).
- [18] G. Quéméner, J.-M. Launay, and P. Honvault, *Phys. Rev. A* **75**, 050701(R) (2007).
- [19] G. Quéméner, N. Balakrishnan, and B. K. Kendrick, arXiv:0811.4377v1 [physics.chem-ph].
- [20] G. Zarur and H. Rabitz, *J. Chem. Phys.* **60**, 2057 (1974).
- [21] J. Schaefer and W. E. Köhler, *Z. Phys. D: At., Mol. Clusters* **13**, 217 (1989).
- [22] P. Diep and J. K. Johnson, *J. Chem. Phys.* **112**, 4465 (2000).
- [23] K. Patkowski, W. Cencek, P. Jankowski, K. Szalewicz, J. B. Mehl, G. Garberoglio, and A. H. Harvey, *J. Chem. Phys.* **129**, 094304 (2008).
- [24] R. C. Forrey, *Phys. Rev. A* **63**, 051403(R) (2001).
- [25] R. C. Forrey, *Phys. Rev. A* **66**, 023411 (2002).
- [26] B. Maté, F. Thibault, G. Tejeda, J. M. Fernández, and S. Montero, *J. Chem. Phys.* **122**, 064313 (2005).
- [27] T.-G. Lee, N. Balakrishnan, R. C. Forrey, P.C. Stancil, D.R. Schultz, and G. J. Ferland, *J. Chem. Phys.* **125**, 114302 (2006).
- [28] R. A. Sultanov and D. Guster, *Chem. Phys.* **326**, 641 (2006).
- [29] R. A. Sultanov and D. Guster, *Chem. Phys.* **428**, 227 (2006).
- [30] D. W. Schwenke, *J. Chem. Phys.* **89**, 2076 (1988).
- [31] A. Aguado, C. Suárez, and M. Paniagua, *J. Chem. Phys.* **101**, 4004 (1994).
- [32] A. I. Boothroyd, P. G. Martin, W. J. Keogh, and M. J. Peterson, *J. Chem. Phys.* **116**, 666 (2002).
- [33] R. J. Hinde, *J. Chem. Phys.* **128**, 154308 (2008).
- [34] D. R. Flower, *Mon. Not. R. Astron. Soc.* **297**, 334 (1998).
- [35] D. R. Flower and E. Roueff, *J. Phys. B* **31**, 2935 (1998).
- [36] D. R. Flower and E. Roueff, *J. Phys. B* **32**, 3399 (1999).
- [37] D. R. Flower, *J. Phys. B* **33**, L193 (2000).
- [38] D. R. Flower, *J. Phys. B* **33**, 5243 (2000).
- [39] S. K. Pogrebnya and D. C. Clary, *Chem. Phys. Lett.* **363**, 523 (2002).
- [40] S. K. Pogrebnya, M. E. Mandy, and D. C. Clary, *Int. J. Mass. Spectrom.* **223-224**, 335 (2003).
- [41] S. Y. Lin and H. Guo, *J. Chem. Phys.* **117**, 5183 (2002).
- [42] F. Gatti, F. Otto, S. Sukiasyan, and H.-D. Meyer, *J. Chem. Phys.* **123**, 174311 (2005).
- [43] F. Otto, F. Gatti, and H.-D. Meyer, *J. Chem. Phys.* **128**, 064305 (2008).
- [44] A. N. Panda, F. Otto, F. Gatti, and H.-D. Meyer, *J. Chem. Phys.* **127**, 114310 (2007).
- [45] G. Quéméner, N. Balakrishnan, and R.V. Krems, *Phys. Rev. A* **77**, 030704(R) (2008).
- [46] M.-M. Audibert, R. Vilaseca, J. Lukasik, and J. Ducuing, *Chem. Phys. Lett.* **31**, 232 (1975).
- [47] W. Bauer, B. Lantzsch, J. P. Toennies, and K. Walaschewski, *Chem. Phys.* **17**, 19 (1976).
- [48] R. V. Krems, TwoBC - quantum scattering program, University of British Columbia, Vancouver, Canada (2006).
- [49] K. Takayanagi, *Adv. At. Mol. Phys.* **1**, 149 (1965).
- [50] S. Green, *J. Chem. Phys.* **62**, 2271 (1975).
- [51] M. H. Alexander and A. E. DePristo, *J. Chem. Phys.* **66**, 2166 (1977).
- [52] A. M. Arthurs and A. Dalgarno, *Proc. R. Soc. A* **256**, 540 (1960).
- [53] B. R. Johnson, *J. Comp. Phys.* **13**, 445 (1973).
- [54] D. E. Manolopoulos, *J. Chem. Phys.* **85**, 6425 (1986).